arXiv:1401.7916v2 [cond-mat.str-el] 19 Dec 2014

Splitting a critical spin chain

Alejandro Zamora,[1] Javier Rodríguez-Laguna,[1,2] Maciej Lewenstein,[1,3] and Luca Tagliacozzo[1]

[1] *ICFO - The Institute of Photonic Sciences, Av. C.F. Gauss 3, E-08860 Castelldefels (Barcelona), Spain*
[2] *GISC & Mathematics Dept., Universidad Carlos III de Madrid, Leganés, Spain*
[3] *ICREA-Institució Catalana de Recerca i Estudis Avançats, 08010 Barcelona, Spain*

We study a quench protocol that conserves the entanglement spectrum of a bipartition of a quantum system. As an example we consider the splitting of a critical Ising chain in two chains, and compare it with the well known case of joining of two chains. We show that both the out of equilibrium time evolution of global properties and the equilibrium regime after the quench of local properties are different in the two scenarios. Since the two quenches only differ in the presence/absence of the conservation of the entanglement spectrum, our results suggest that this conservation plays a fundamental role in both the out-of-equilibrium dynamics and the subsequent equilibration mechanism. We discuss the relevance of our results to the next generation of quantum simulators.

I. INTRODUCTION

The dynamical evolution of an isolated quantum system is governed by a unitary operator and is, consequently, reversible. Therefore, one might think that irreversibility and thermalization should only appear through the system-environment interaction [1]. For a small region inside a large isolated quantum system, a legitimate environment is the system itself. In particular, it is important to understand, under which conditions the large-time out of equilibrium evolution of an isolated system will lead to a thermal state of the small region. Although the decoherence time of most experimental systems is too short for an effective study of that regime, recent advances in cold atomic physics [2] have allowed to experimentally address such situations and have boosted renewed interest in the theoretical understanding of these phenomena [3–7]. The experiments have been complemented with theoretical insights [8–11], which have brought about interesting ramifications of the problem, ranging from quantum information and entanglement to the issue of integrability in quantum systems.

In the context of the low energy physics of a many body quantum systems, entanglement has emerged as a privileged tool to characterize quantum phases. In 1D, for example, the scaling of entanglement allows to distinguish between gapped systems and critical systems, and the structure of the entanglement spectrum allows to identify symmetry protected topological phases. Here we try to analyze the effects of the conservation of the entanglement in the out-of-equilibrium evolution after a quantum quench.

Conserved quantities play a very special role in Physics. In classical mechanics, they allow to define integrable systems as those systems that possess as many conserved quantities as degrees of freedom. In quantum mechanics, this concept is hard to generalize. The expectation value of any operator that commutes with the system Hamiltonian is conserved. In particular, arbitrary powers of the Hamiltonian itself (that in general can define independent operators) are conserved during the out-of equilibrium dynamics. This means that a generic quantum system possesses as many conserved quantities as degrees of freedom, and we still miss a proper definition of integrable quantum systems.

Furthermore, when considering *local equilibration*, the equilibration of a small region inside a large quantum many body system, among all conserved quantities, only few seem to be relevant. For example when a generic quantum many body system locally relaxes, it does it to a thermal state and thus the only *relevant* conserved quantity is the expectation value of the energy. Indeed the Gibbs ensemble (or thermal state) is formally obtained by maximizing the entropy at fixed value of the energy [12–14]. Exactly solvable systems, can still locally equilibrate, but to more complex ensembles obtained by maximizing the entropy subject to the constraints arising from the conservation of all relevant quantities. It is still unclear in general how to identify the relevant conserved quantities, but in the cases where they are known, the ensembles that describe the equilibrium of small regions are called generalized Gibbs ensembles (GGE) [15, 16].

Is entanglement one of those relevant conserved quantities? In order to understand this we address the non-equilibrium dynamics arising after a *quantum quench* [9]. The system is originally in the ground state of a certain Hamiltonian H_0. One suddenly quenches the Hamiltonian from H_0 to H and observes the subsequent out of equilibrium dynamics. Depending on if H differs from H_0 locally (on few sites) or globally (on the whole system) quenches are called *global* or *local*. In particular, we characterize the quench obtained by *splitting* a critical spin chain into two equal halves. This amounts to turning off at $t = 0$ the interaction between the two half chains. This, together with the fact that the evolution inside each of the two halves is unitary, implies that the original entanglement between them is conserved during the evolution. Thus, the initial correlations between the two halves are expected to survive along the whole evolution.

A similar phenomenon was observed already in the experiments carried out by Gring and coworkers in Vienna [5], where a quasi-1D Bose gas was split into two halves.

The two halves were subsequently allowed to evolve independently. After a time shorter than the expected equilibration time, many of the observables had relaxed, a phenomenon usually called *prethermalization* [17, 18]. After the prethermalization, the evolution was much slower, and compatible with the effects of the heating of the system due to the residual small interactions with the environment. Nevertheless, the original almost stationary interference pattern between the two halves persisted for large times after the prethermalization time. In a truly isolated system this would have been there forever as a consequence of the initial entanglement between the two halves. A truly isolated quantum system, indeed, conserves the initial entanglement between two systems that are separated and stop interacting. While it is clear, that by splitting the system one initially injects into the system an amount of extra energy that is proportional to the geometry of the splitting (extensive in the Vienna experiment and intensive in the case we consider here) and thus generate the subsequent out-of-equilibrium dynamics, it is not clear what is the role of the conservation of the entanglement in the subsequent equilibration process.

From a quantum information perspective, the key insight is that not only the entanglement is conserved, but also each of the individual eigenvalues of the reduced density matrix of any of the two separated regions is conserved. All together they constitute the entanglement spectrum (ES) [19]. How does this large amount of constraint affect the dynamics?

In order to address this point, we compare the non equilibrium dynamics generated by two similar quenches. We either split a critical spin chain into two halves (we will refer to this situation as to the *split quench*), or we join two critical chains in a larger one (and we will refer to this scenario as to the *join quench*). Both scenarios are local quenches. Initially, in the bulk, in middle of the two regions that are either split or joined, any correlation function of local observables (once appropriately rescaled) is the same in the two cases. Also the post-quench Hamiltonian is the same in the bulk for both quenches. We thus say that the two quenches are in the bulk initially "locally" indistinguishable. They are clearly distinguishable close to the boundaries of the sub-systems. While the split quench conserves the initial correlations between the two halves, the join quench does not since the interaction between the two halves allows to distribute correlations among them along the evolution.

The main result that we present here, is that the out-of-equilibrium dynamics and the subsequent relaxation of the bulk of the two systems are distinguishable, and, thus, the presence/absence of conservation of the entanglement spectrum affects the out of equilibrium dynamics of the system (for related ideas see also Ref. [20]).

This article is organized as follows. Section II introduces some general concepts and notation regarding quenches and thermalization. It also presents our quench protocol and the concrete model we consider, the Ising model in a transverse field (ITF). Section III A analyses the entanglement structure of the initial state, and discusses its possible effects on the subsequent dynamics. In the rest of section III we explore the time evolution of different characteristic magnitudes: the entanglement entropy of different types of blocks, correlation functions —both within the same half and across the split—, and local magnetization. The final section, IV is devoted to summarizing the main conclusions and discussing further work.

II. THE SPLITTING QUENCH

A. Quenched dynamics and thermalization

The state $|\phi_0\rangle$ is the ground state (GS) of a certain closed system described by the Hamiltonian H_0. A quench is performed by changing abruptly the Hamiltonian from H_0 to H, in such a way that $|\phi_0\rangle$ ceases to be an eigenstate, and thus undergoes non-trivial unitary evolution

$$|\phi(t)\rangle = \exp(-iHt)\,|\phi_0\rangle\,. \tag{1}$$

A is a (small) region of the system, containing $r \ll N$ spins, described by the reduced density matrix $\rho_A(t) = \mathrm{Tr}_B\,|\phi(t)\rangle\,\langle\phi(t)|$, where B is the complement of A. Under certain conditions [21–23, 29], the limit $\bar{\rho}_A \equiv \lim_{t\to\infty}\rho_A(t)$ exists, i.e., for large enough times, the region A equilibrates to a stationary state. Typically, a certain amount of time-averaging is necessary in order to remove small fluctuations.

If, at equilibrium, the state of A is well described by a thermal state, it means that, for the equilibration process, the only relevant conserved quantity is the energy E. The thermal state is indeed given by $\bar{\rho}_A \simeq \mathrm{Tr}_B \exp(-\beta H)$, where β is chosen such that $\mathrm{Tr}(H\rho_A)/\mathrm{Tr}(\rho_A) = E$. If the Hamiltonian is known to commute with a larger set of relevant local observables, $\{\langle H_i\rangle\}_{i=1}^K$, the equilibrium state is a generalization of the thermal state, $\bar{\rho}_A \simeq \mathrm{Tr}_B \exp(-\sum_{i=1}^K \beta_i H^i)$ and is called a *Generalized Gibbs ensemble* [16, 24].

B. The quench protocol

Consider a spin-chain of length N, described by a local homogeneous Hamiltonian with open boundary conditions, H_0, which can be formally decomposed into three terms:

$$H_0 = H_L + H_R + H_{LR}. \tag{2}$$

where H_L and H_R act, respectively, on the left and right halves, and H_{LR} represents the term connecting them.

We prepare the system in its ground state, $|\Omega_0\rangle$, and proceed to quench the Hamiltonian to

$$H_t \to H = H_L + H_R, \tag{3}$$

i.e., we remove the connecting term, H_{LR}. The upper panel of Fig. 1 illustrates the procedure.

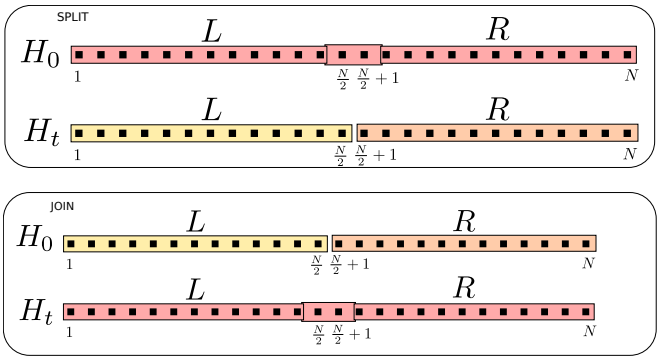

Figure 1. Upper panel: *Splitting a spin chain.* After the ground state of a spin-chain of length N has been obtained, the Hamiltonian is quenched by removing the term which connects both halves, effectively splitting them. Lower panel: *Joining two spin chains.* The situation is reversed, the ground states of two separate chains are quenched by adding the missing term in the Hamiltonian which connects them. This provides a reference quench for comparison since the two quenches are locally indistinguishable and only differ by the presence/absence of the conservation of the entanglement spectrum.

The state now evolves as

$$|\phi(t)\rangle = \exp(-iHt)\,|\Omega_0\rangle\,. \tag{4}$$

The initial state $|\Omega_0\rangle$ has excess energy with respect to the ground state of the new Hamiltonian H, $|\Omega_L\rangle \otimes |\Omega_R\rangle$. This excess energy can be interpreted as the presence at $t = 0$ of a finite density of quasi-particles located at the junction between L and R [27]. If H is a sum of local terms, these quasi-particles will propagate with a finite speed, giving rise to the characteristic light-cone effects observed in local quenches [4]. Of course, if H contains long-range interactions, this behavior can differ [28, 30].

The left half of the system L, at time $t = 0$, is described by a mixed state, obtained by the following reduced density matrix

$$\rho_L(0) = \mathrm{Tr}_R\,|\Omega_T\rangle\,\langle\Omega_T|\,. \tag{5}$$

that can be diagonalized as,

$$\rho_L(0) = \sum_{\alpha=1}^{m} \lambda_\alpha\,|\chi_\alpha\rangle\,\langle\chi_\alpha| \tag{6}$$

where m is the Schmidt rank, and the orthonormal $\{|\chi_\alpha\rangle\}$ are called Schmidt vectors. The subsequent time evolution of $\rho_L(t)$ will be given by

$$\rho_L(t) = U_L(t)\rho_L(0)U_L^\dagger(t) \tag{7}$$

where $U_L(t) = \exp(-iH_Lt)$. An immediate consequence is that the spectrum of $\rho_L(t)$, the set of $\{\lambda_k\}_{k=1}^m$, is preserved by the evolution. The Schmidt vectors, nonetheless, evolve in a non-trivial way, describing a time dependent set of orthogonal vectors. At any later time indeed,

$$\rho_L(t) = \sum_{\alpha=1}^{m} \lambda_\alpha\,|\chi_\alpha(t)\rangle\,\langle\chi_\alpha(t)| \tag{8}$$

with the same set of $\{\lambda_k\}_{k=1}^m$ than the one in Eq. 7. It is customary to describe $\rho_L(0)$ in terms of a certain entanglement Hamiltonian $\mathcal{H}_L$, such that $\rho_L(0) = \exp(-\mathcal{H}_L)$ [19], i.e., as if it were a thermal state at an effective temperature $\beta = 1$. The entanglement spectrum (ES) is defined to be the set of eigenvalues of $\mathcal{H}_L$, $\epsilon_\alpha = -\log(\lambda_\alpha)$. Thus, as a consequence of the conservation of the eigenvalues of ρ_L, the ES between the left and right parts is also conserved.

How does in general change the local equilibration after a quench when the ES is conserved? In order to address this question we can study the equilibration of a generic mixed state constructed from a set of orthogonal vectors $|\phi\rangle_\alpha$ each appearing with probabilities λ_α. We can perform the time evolution for each of the state individually (it is a linear map) and then reconstruct the appropriate mixed state by summing the result with the appropriate probabilities. In the simplest scenario we can assume that each of the vectors $|\phi\rangle_\alpha$ fulfills the necessary conditions for thermalization described in Ref. [22]. Depending on the initial energy of each them E_α, they will locally thermalize to the corresponding temperatures β_α such that $\mathrm{Tr}(H\exp(\beta_\alpha H))/\mathrm{Tr}(\exp(\beta_\alpha H)) = E_\alpha$. If the β_α obtained in this way are not sufficiently close, the final state can not be described by a single temperature. Similarly, if there are more preserved quantities, the final state will not be uniquely determined by their initial expectation values. The final state might, therefore, not be described by a Gibbs (or generalized Gibbs) ensemble. In other words, the system would not locally thermalize in the usual sense but it would equilibrate to an exotic ensemble.

Is this non-thermalization likely to occur for the initial mixed state obtained in the split quench? A generic scaling argument suggests that such temperature mixing is difficult to achieve. Ground states of gapped 1D Hamiltonians fulfill the area law of entanglement [25, 26]. This implies that the number of Schmidt vectors saturates with the system size in the thermodynamic limit. The temperature mixing effect might be more relevant for a critical initial state, for which the number of Schmidt vectors scale as a power law of the system size [47]. Still

different Schmidt vectors, typically only differ locally so that their initial energies are very similar. We thus do not expect to observe the temperature (or generalized parameter) mixing in our setting. Still, in the results we present, we will observe some remnants of the fact that the ES is conserved.

In order to clarify the role of the ES-conservation, we will compare the splitting quench with the joining quench of the same spin-chain, as illustrated in the lower panel of Fig. 1. In this last case, one first obtains the ground state of H_t in Eq. (3) and then quenches the Hamiltonian by adding the connecting term H_{LR}, i.e.: applying H_0. This effectively joins the two independent chains. This case has been addressed both at criticality and away from it using several techniques, which range from conformal field theories (CFT) to free fermions [31–33].

Since both quenches are locally described by the same Hamiltonian, and the correlation functions of any local operator, in the bulk of the initial states, are indistinguishable, we might expect that the difference between the corresponding out-of-equilibrium evolutions should be negligible far away from the division between L and R. We will show that this is not the case, and the two quenches produce substantially different states, both globally and —more interestingly— also locally.

C. The critical Ising chain

As a prototypical example, let us consider the Ising model in transverse field (ITF), a simple integrable one-dimensional spin-chain,

$$H_0 = -\sum_{i=1}^{N} \left[\sigma_i^x \sigma_{i+1}^x + \Gamma \sigma_i^z\right]. \tag{9}$$

where i ranges over the N sites of a 1D lattice and σ^x and σ^z stand for the Pauli matrices. The model presents two phases: a X-polarized phase for $\Gamma < 1$ and a Z-polarized phase for $\Gamma > 1$. They are separated by a second-order phase transition at $\Gamma_c = 1$, where we will perform all our calculations. The ITF can be rewritten as a free-fermion model via a Jordan-Wigner and a Bogoliubov transformation [34]

$$H_0 = \sum_k \epsilon_k \left(\eta_k^\dagger \eta_k - \frac{1}{2}\right) \tag{10}$$

with $\eta_k^\dagger$ and η_k following the usual anticommutation relations. The model is, therefore, integrable, and all its conserved quantitites can be expressed as a function of the mode occupations n_k [24]:

$$n_k = \langle \Omega_T | \, \eta_k^\dagger \eta_k \, | \Omega_T \rangle . \tag{11}$$

The low-energy physics of the ITF model close to the phase transition and its out-of-equilibrium dynamics can also be described using CFT [31, 32, 35].

In this work we have studied the two quenches via both free-fermion techniques [36] and the *time evolving block decimation* (TEBD) method, based on matrix product states (MPS) [37, 38]. MPS techniques have the advantage that they can be extended to both interacting models and non-integrable models.

III. NUMERICAL RESULTS

We first analyse the relation between the Schmidt vectors of the initial state and the eigenvectors of the post quench Hamiltonian H. This gives us the opportunity to understand better the possible connections between the conservation of the entanglement spectrum and the long-time equilibrium regime. As we have discussed, the distribution of the expectation value of the energy and all relevant conserved quantities taken on the set of the Schmidt vectors are the ultimate quantities that determine if the system equilibrates to a well defined GGE ensemble or not.

We then will proceed to a more traditional characterization of the states resulting from the split quench focusing on two types of properties, global and local. Among the global properties, we will consider the entanglement entropy of different types of blocks and large-distance correlation functions. The local properties are characterized by studying the expectation values of local operators.

The entanglement entropy of a block A, with reduced density matrix ρ_A, is defined as

$$S_A = -\mathrm{tr}\rho_A \log \rho_A. \tag{12}$$

We consider both the case in which A is completely contained in one of the two blocks (say L) and when it is shared in between L and R, see Fig. 6.

With respect to correlation functions, we will evaluate the two-point correlation function of the order parameter, defined as

$$\begin{aligned} C(r_1, r_2, t) = &\langle \varphi(t) | \sigma_x(r_1) \sigma_x(r_2) | \varphi(t) \rangle \\ &- \langle \varphi(t) | \sigma_x(r_1) | \varphi(t) \rangle \langle \varphi(t) | \sigma_x(r_2) | \varphi(t) \rangle . \end{aligned} \tag{13}$$

In particular, we will consider distances $|r_1 - r_2|$ scaling with the size of the system, $|r_2 - r_1| \propto N$, in order to study the thermodynamic limit. Since both the splitting and the joining quenches break the translation invariance explicitly, we will consider separately the cases in which both r_1 and r_2 are on the same side with respect to the splitting point, or when they lie in different sides.

All those properties will be studied as a function of time. We will also focus on the equilibrium regime which emerges after the transient out-of-equilibrium dynamics.

Although global properties, as discussed in the introduction, do not equilibrate, in a local quench we can still observe equilibration of an extensive region A that nevertheless should be separated from the boundaries. Indeed, in our simulations, we always observe three different regimes: (i) the static, (ii) the out-of-equilibrium regime and (iii) the equilibration regime, see Fig. 2. This fact is well understood by the approximate picture of the radiation of quasi-particles introduced by Cardy and Calabrese [27]. Indeed, through a local quench, one typically populates all single quasi-particle momentum states with equal probability, which then propagate outwards with finite speed v.

Since our model is described at low energy by a CFT, all pseudo-particles propagate with the same speed at first order in $1/N$. In this paper we will not address the corrections to this picture, that i.e. for long times, are responsible for the spread of the pesudo-particles and thus spoil the periodicity of the dynamics.

The out-of-equilibrium evolution of a region A which lies at a distance d from the interface between L and R will start after a time $t_1 \approx d/v$. For earlier times, a *static* regime is observed. Eventually, at a time $t_2 > t_1$ the slowest particles leave the region and the *equilibration* regime begins. Due to the finite size of the chains, if we wait for a large enough time $t_N \gg t_2$, the quasi-particles will bounce back at the boundary and return to the region A, thus making the system depart from equilibration. Thus, we will search for the equilibration regime in the time window $t_2 \gg t \gg t_N$, which depends on the distance from A to the boundaries and the velocities of the different types of quasi-particles. For times $t \gg t_N$ the behavior of the system is plagued with finite-size effects, which we want to avoid since we are interested in the thermodynamic limit. This implies that we can consider at most times of the order of t_N.

When addressing local properties, the static regime is followed by a very fast relaxation which leads to the equilibration regime. This can be readily explained assuming that times t_1 and t_2 coincide.

A. Schmidt vectors of the initial state

We want to understand the relation between each of the Schmidt vectors and the expectation value of the observables that are conserved during the time evolution. We start with the energy. We arrange the eigenvalues of the reduced density matrix $\rho_L(0)$, $\{\lambda_\alpha\}$, in decreasing order. In this way we can define an effective *energy gap* as

$$\Delta E_L = \langle \chi_2 | H_L | \chi_2 \rangle - \langle \chi_1 | H_L | \chi_1 \rangle \qquad (14)$$

We find numerically that ΔE_L decays as a power of the logarithm of the system size, as shown in Fig. 3. The appearance of a logarithmic scaling could be related with the results of [40–43], that establish a mapping between

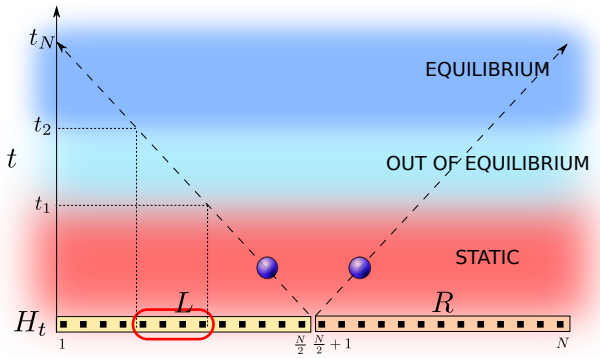

Figure 2. *Relevant time scales:* During the out-of-equilibrium evolution which follows the split quench, the region A is characterized by three different regimes as a consequence of the finite speed at which the quasi-particles created at the junction between L and R radiate. A *static* regime, lasting up to time t_1, in which the behavior is almost unchanged. This time t_1 is indeed the time necessary for the fastest quasi-particle to reach the region. After t_1, A experiences an *out-of-equilibrium* regime up to a certain t_2, the time needed by the slowest quasi-particles to travel through A and abandon it. From t_2 up to t_N, we observe *the equilibration* of the region. At t_N, the fastest quasi-particles bounce back from the boundaries so that finite size effects start to play a dominant role.

the reduced density matrix of the ITF and the transfer matrix of the corresponding classical model on a cylinder whose radius grows logarithmically with the size of the block.

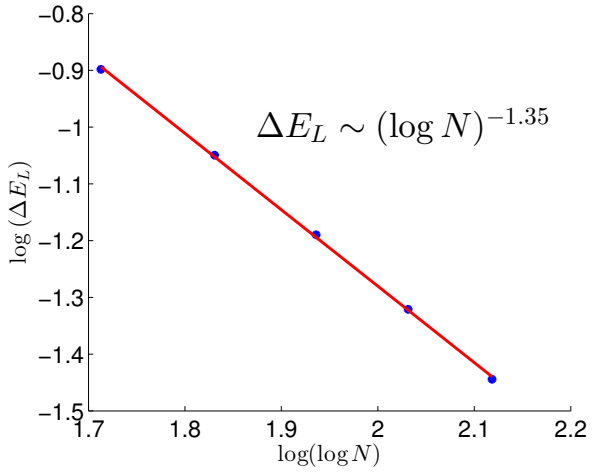

Figure 3. Energy gap ΔE_L between the first two Schmidt vectors of the left half of a critical Ising chain as a function of the chain length. The data suggest that the gap closes as a power of the logarithm of the system size.

The mode occupations 11 for the first three Schmidt vectors are presented in the main panel of Fig. 4. They resemble Fermi-Dirac distribution functions at low temperature, and it is possible to identify a certain Fermi level that discriminates between almost fully and almost

empty modes. Nonetheless, the occupations near the Fermi level differ considerably among different Schmidt vectors, as shown in the left inset of Fig. 4. Those differences decrease slowly as a power law of the system size (see Fig. 4, right inset).

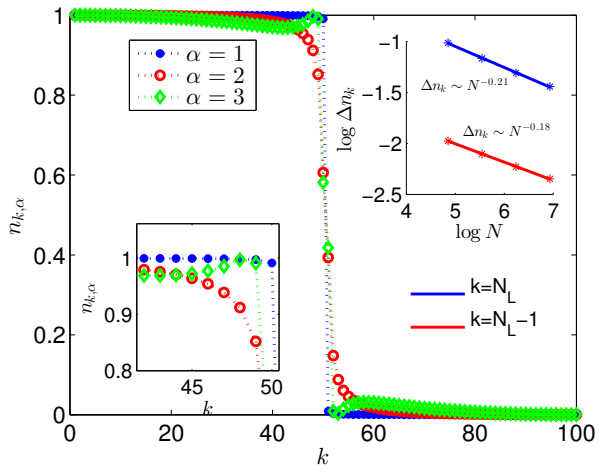

Figure 4. Main panel: occupation numbers of the modes of Hamiltonian H_L for the first three Schmidt vectors, for chains with $N = 100$ spins. Left inset: the differences in occupation are more pronounced around the Fermi energy. Right inset: Those differences scale as a power of the system size.

The Ising model can be mapped to free fermions and thus all conserved charges are functionally dependent on the mode occupations. Since for each Schmidt vector the mode occupations are different this suggests that this type of quench could provide an example of equilibration to a strongly correlated state that differs both from the Gibbs and the Generalized Gibbs Ensembles (GGE), as opposed to what is expected for standard quenches.

A more careful quantitative analysis, however, shows that this is not the case. Indeed, the fluctuations of the energy in the initial state are not large enough to produce significant effects on the equilibration state. As shown in Fig. 5, those fluctuations are independent of the system size, so that in the thermodynamic limit they vanish as $1/N$ (inset).

This is not surprising since, in a local quench, the initial state of the system does not possess enough energy to equilibrate to a thermal (or generalized thermal) state characterized by an extensive scaling of the entanglement entropy of a region. Indeed, in the initial state of a local quench, the excess energy density with respect to the ground state scales with $1/N$, and thus it is not surprising that also its fluctuations scale as $1/N$. This implies that the equilibrium state of a local quench is very close to a zero temperature state where, for critical systems, the entanglement entropy of a region only grows logarithmically with its size [44–48]. Still, as we will see in the following, the conservation of the entanglement spectrum has non-trivial consequences both on local and

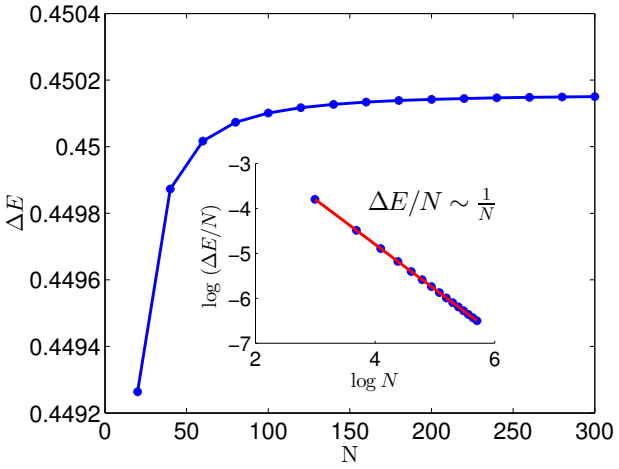

Figure 5. Main panel: Energy fluctuations as a function of the system size. We see that local fluctuations (inset) decay to zero as $1/N$, as expected in the case of a local quench.

global properties of the system.

B. Entanglement entropy

The time evolution of the entanglement entropy has been computed analytically in a few selected settings [27, 31, 32, 35, 49], and numerically in many others, local or global quenches, impurities or disorder [33, 50–55].

In this section we analyze the time evolution of the entanglement entropy of a block A of size $r < N$, as defined in Eq. 12, for two different geometrical configurations (see Fig. 6), A may have (i) a single active boundary or (ii) two of them. In this second case, the two boundaries may lay on different parts (ii.a) or on the same part (ii.b) of the splitting point.

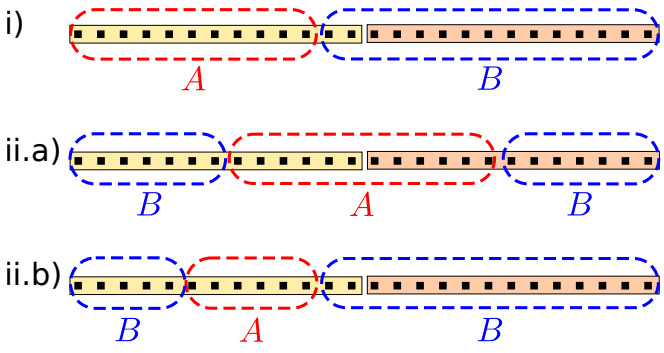

Figure 6. The geometrical configuration of block A within the full chain, (i) A has only one active boundary; (ii.a) A has two active boundaries, one in L and the other in R; (ii.b) the two active boundaries are both inside L.

Fig. 7 is devoted to the analysis of entanglement in configuration (i). Let A be formed by the leftmost r sites of a chain with $N = 160$ spins, split into two halves.

The upper panel of Fig. 7 shows the entanglement entropy $S(r,t)$ as a function of both the size of the block (X-axis, marked r), and time in units of $1/J$ (Y-axis, marked t $(1/J)$). Notice that, since the entanglement Hamiltonian of the left part, $\mathcal{H}_L$, is a constant of motion, $S(N/2,t)$ is preserved during time evolution. At $t=0$, S_r presents the characteristic shape of a critical system: $S(r,0)=\frac{c}{6}\log\left(\frac{L}{\pi}\sin\left(\frac{\pi l}{L}\right)\right)$ [44–48]. But for further times, a light-cone develops at the LR interface, and the entanglement entropy only changes when the fastest quasi-particles generated at the quench cross the active boundary of A as a specific case of the cartoon sketched qualitatively in Fig. 2.

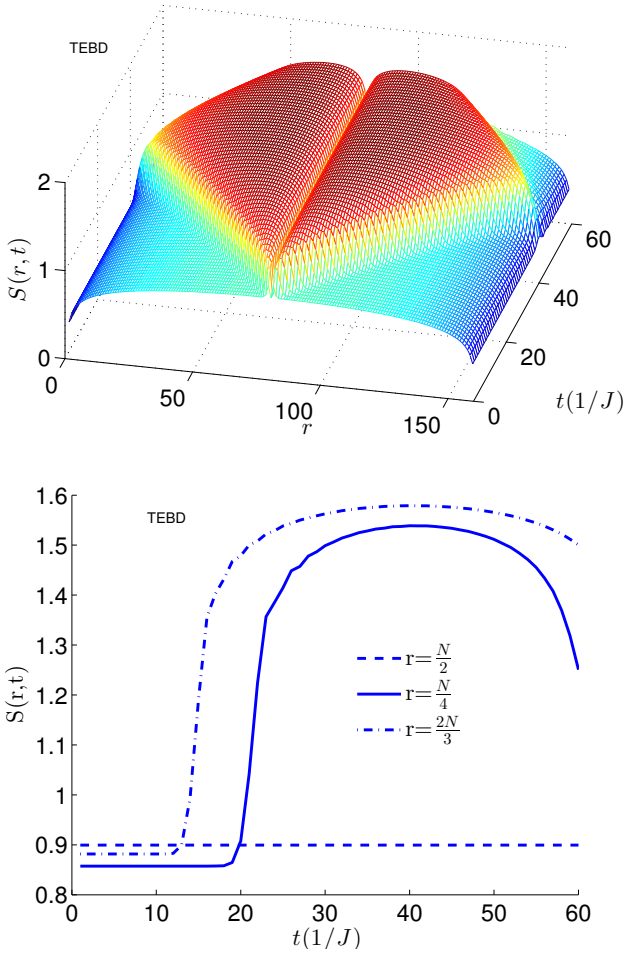

Figure 7. *Upper panel:* Time evolution of the entanglement entropy $S(r,t)$ for a chain of $N=160$ after the splitting. *Lower panel:* Time evolution of $S(r)$ for three different values of r. When $r=N/2$, entropy remains constant. In the other two cases, entropy starts to grow only after the fastest quasi-particles enter (if $r<N/2$) or leave (if $r>N/2$) the block.

The lower panel of Fig. 7 shows the time evolution of S for blocks of type (i) and different sizes. $S(N/2,t)$ is constant; $S(N/4,t)$, has a single active boundary that lies at the left of the splitting point, and thus it presents a stationary behavior for short times followed by a fast increase when the quasi-particles reach $N/4$; we also analyze $S(2N/3,t)$, whose active boundary lies to the right of the split point. In this case quasi-particles are radiated from within the region and only contribute to an increasing entropy when they leave the region.

From the space-time diagram of the upper panel of Fig. 7 we can extract two projections. A time-like projection $\tilde{S}_T(t)$ is obtained by finding, for each time t, the maximal entropy among all block-sizes, and a space-like projection $\tilde{S}_S(r)$ defined by finding, for each block-size, the maximal entropy achieved along the evolution. After a joining quench, the time-like projection $\tilde{S}_T$ only grows logarithmically with time [32, 50]

$$\tilde{S}_T(t)=\frac{c}{3}\log_2\left|\frac{N}{\pi}\left(\sin\frac{\pi v t}{N}\right)\right|+\text{cst}$$

where $c=\frac{1}{2}$ is the central charge of the critical Ising chain and v is the quasi-particle velocity. The space-like projection, $\tilde{S}_S(r)$ is described by the same equation, just replacing t with r. On the other hand, after a splitting quench, $\tilde{S}_T(t)$ behaves as

$$\tilde{S}_T(t)=\frac{c}{3}\log_2\left|\frac{N}{\pi}\left(\sin\frac{\pi v t}{N}\right)^{1/2}\right|+\text{cst}, \qquad (15)$$

where the main difference with the result for the joining quench is the presence of the square root (see upper panel of Fig. 8). The space-time projection $\tilde{S}_S(r)$ presents a cusp at $r=N/2$ which is absent in the joining case. Still, for small r, the two cases are difficult to distinguish (see lower panel of Fig. 8). The detailed analysis is presented in Appendix A.

The block in configurations (ii) in Fig. 6 have two active boundaries. As discussed previously, we distinguish between blocks (ii.a) which overlap with both parts, which we will place centered on the LR interface, and (ii.b), those which lie totally within one part. In Fig. 9 we consider two blocks of size $r=8$, one of them centered on the LR interface (ii.a) and the other at a distance $l=10$ from it. Notice that the time evolution of the entropy of two blocks presents the three aforementioned stages: static, out-of-equilibrium and equilibrium. In both cases, at large times the entropy converges to a finite value S_{eq}.

In the joining quench the relaxation towards S_{eq} is governed by [33]

$$S(r_0,t)=S_{eq}+\frac{\alpha\ \log(t)+\beta}{t}, \qquad (16)$$

where the parameters α and β depen on the distance l between the block and the site of the quench.

The insets of Fig. 9 unveil a leading behavior of the same type as Eq. 16 with superimposed oscillations and faster time scales.

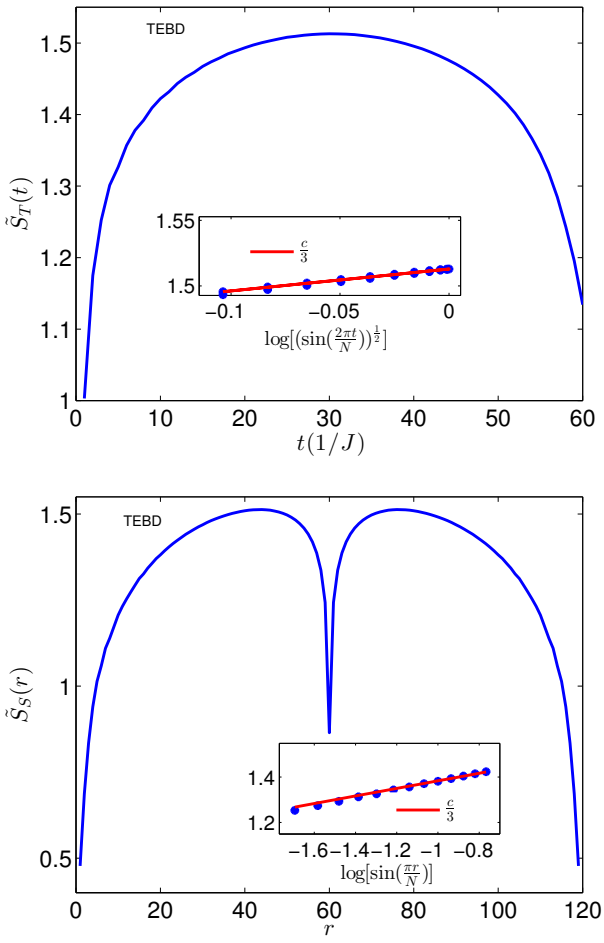

Figure 8. *Upper panel:* Time-like projection of the entropy, $\tilde{S}_T(t)$, after a splitting quench. The inset shows that the growth is compatible with a logarithmic growth with a pre-factor close to $\frac{c}{3}$, as in the join quench, but with an extra square root inside the logarithm (see Eq. 15). *Lower panel:* Space-like projection, $\tilde{S}_S(r)$. For block sizes very different from $N/2$, it behaves as in the join quench, displaying a logarithmic growth with a pre-factor close to $\frac{c}{3}$.

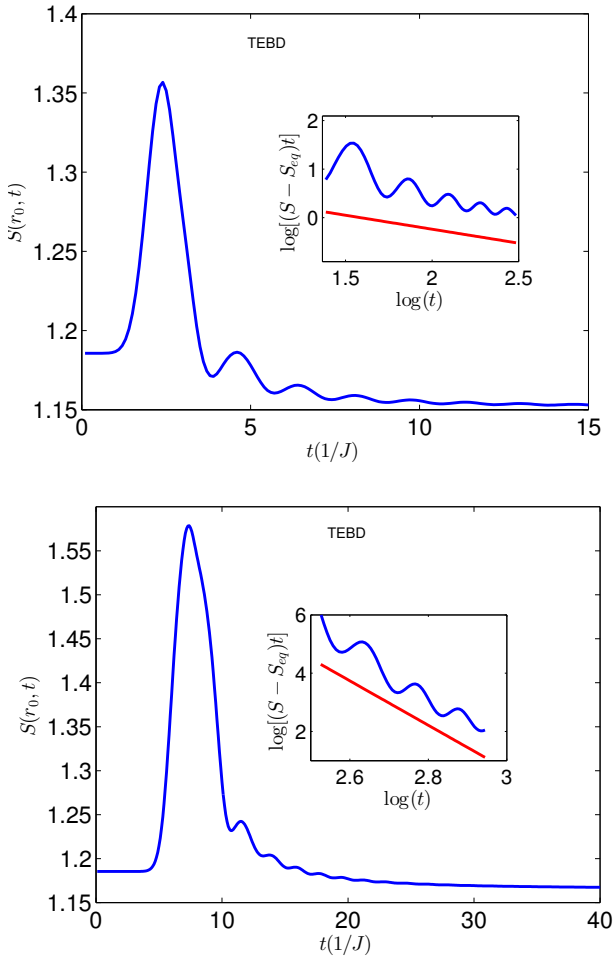

Figure 9. *Upper panel:* Time evolution of the entanglement entropy for a block with $r_0 = 8$ sites centered on the LR interface in a spin-chain of $N = 160$ sites. Notice the sudden jump to a maximum value and the slower relaxation towards S_{eq}. *Lower panel:* Same evolution, but for a block with $r_0 = 8$ sites, located at a distance $l = 10$ from the interface. In both cases the insets show that the relaxation behavior is compatible with the one of Eq. 16, as in the case of the joining quench, but with faster timescales and super imposed oscillations.

The entanglement spectrum of a block in configuration (i) of Fig. 6 presents only the first two out of the three time regimes, static and out-of-equilibrium. This is a consequence of the fact that the block extends up to the extreme of L and the quasi-particles never have space to escape. The Schmidt coefficients of the reduced density matrix of a block increase abruptly when the quasi-particles reach the block, and slower further increase afterwards. During this last regime, the Schmidt coefficients λ_α^r decay as a power of α (see lower panel of Fig. 10), pointing to the possibility of approximating the state by keeping only a small number of them, χ. The error of this approximation, which is the usual systematic error of MPS-based techniques, is given by

$$\epsilon = 1 - \sum_{\alpha=1}^{\chi} (\lambda_\alpha^r)^2. \qquad (17)$$

The lower panel of Fig. 10 shows also the Schmidt number χas a function of time required to achieve two possible desired tolerances ϵ. Notice that the value of χ increases only moderately during the whole time interval, justifying our choice to use the TEBD algorithm [56].

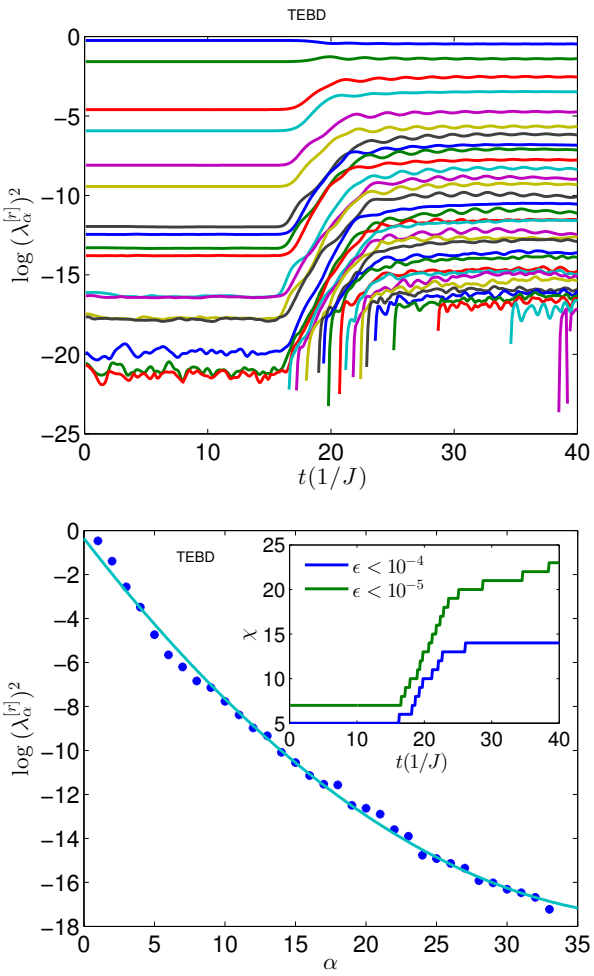

Figure 10. *Upper panel:* Time evolution after a split quench of the entanglement spectrum for a block of type (i) with size $N/4$ in a chain of length $N = 140$. Notice that only two time regimes are present: static and out-of equilibrium. *Lower panel:* After the fast increase ($t = 40$), the entanglement spectrum decays polynomially, showing that the state is neatly approximable with a few Schmidt vectors, χ. Small values of the representation error are obtained with $\chi \approx 20$, as shown in the inset.

C. Correlation functions

Let us turn to the time evolution of the two-point correlation functions of the order parameter after splitting the chain, defined in Eq. 13, and compare them with the joining case, which has been studied in detail by several authors [31, 57]. As with the entanglement entropy, we will study them in two geometric configurations, shown in Fig. 11, when both sites r_1 and r_2 are in different halves of the chain (top panel) and when they lie in the same half (bottom).

In the static regime, since the system is critical, for $|r_2 - r_1| \propto N$, $C(r_1, r_2, t) \propto N^{-2x}$ with $x = 1/8$ (see Fig. 14, both panels, for short times).

Let d_1 and d_2 be the distances from both points

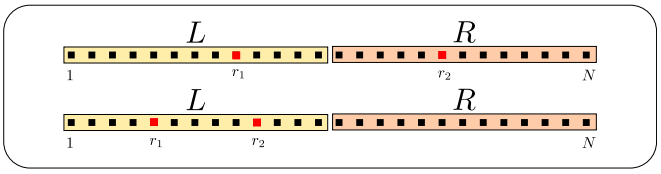

Figure 11. *The two-point correlation function of the order parameter,* defined in Eq. 13, is studied in two different configurations, when the two sites are on different halves (top) and when they lie on the same half (bottom) of the split chain.

to the LR interface, $d_{\min} = \min(d_1, d_2)$ and $d_{\max} = \max(d_1, d_2)$. The out-of-equilibrium regime is defined by the condition $d_{\min} < vt < d_{\max}$, i.e.: the time lapse in which the quasi-particles have already reached the closest point and have not yet left the region between the two points. In the time-regime where $d_{\min} < vt \ll d_{\max}$, the CFT predicts that after a joining quench the correlation function will behave as $C \propto d_{\max}^{-2x-1/2}$ [31], independently on whether the points are in the same or different halves. This prediction has been confirmed numerically [57]. Fig. 12 shows the results in our case. After the split quench, when the points are in the same half, we also observe $C \propto d_{\max}^{-\alpha}$, but with $\alpha \approx 1/2$ ($\alpha = 0.46(5)$). Generalizing the CFT prediction, we may write this as $C \propto d_{\max}^{-2x-1/4}$. In the case of points in different halves, we do not observe any power law decay in the correlation function, as shown in the lower panel of Fig. 12.

We study next a kind of *light-cone regime* by fixing the ratios $\epsilon(t) = \frac{d_{\min}}{vt} < 1$ and $R(t) = \frac{d_{\max}}{vt} > 1$. In the joining quench, the correlation in this regime is described by $C \propto t^{-3x}$ as $t \to \infty$ [57]. Our results for the split quench are shown in Fig. 13. We can observe also a power law decay of correlations as in the joining case but when both points are located in the same half of the chain the exponent we extract is 0.46(1) that apparently is not compatible with the joining case. Interestingly, when they lay in different halves, we still observe a polynomial decay of the correlations with t, but with the exponent close 3/4, 0.72(1), that doubles the one observed in the joining case.

Finally, we reach the equilibrium regime. If both points lie on the same half, correlations decay as a power law of the system size, as in the joining quench as shown in the inset of the upper panel of Fig. 14. This means that the system is still critical, with the same critical exponent $x = 1/8$, and has thermalized to a temperature which is very close to zero. If the points are on different halves we still observe power-law behavior but this time we observe anti-correlations that decay with the same critical exponent $x = 1/8$, as shown the inset in the lower panel of Fig. 14.

D. Local properties

As we have seen, the evolution of global quantities after the split quench is very different from the one after

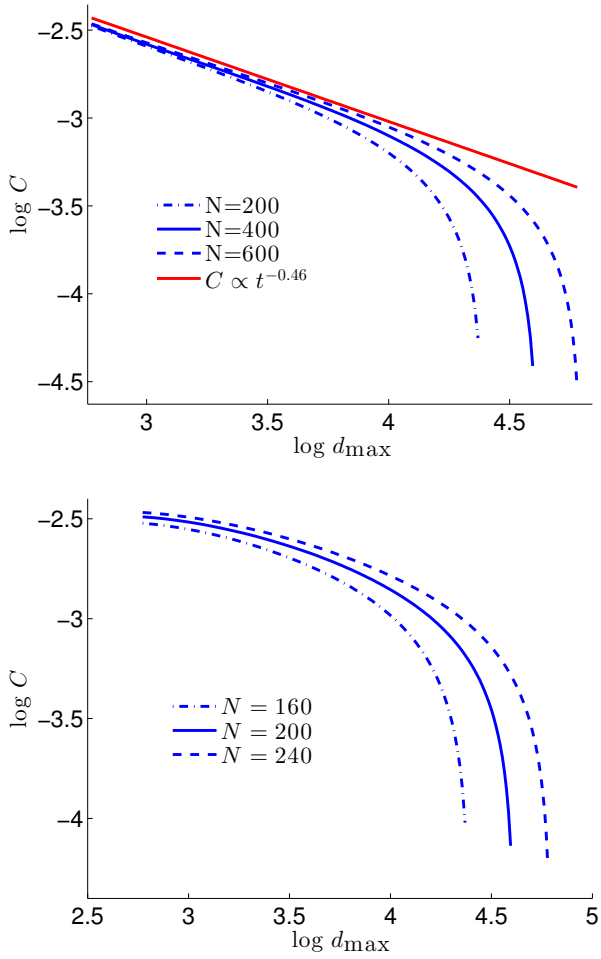

Figure 12. *Correlations in the out-of-equilibrium regime.* Both panels show the correlations in the time window $d_{\min} < vt \ll d_{\max}$, as a function of $d_{\max}$. The upper panel considers the case in which both points lie in the same half, showing a power-law decay with $d_{\max}$. The lower panel considers the case in which the two points lie in different halves, showing no power-law behavior. In both cases, we have considered $d_{\min} = 1$, $16 < d_{\max} < N/2$ and $t = 3$ $(1/J)$.

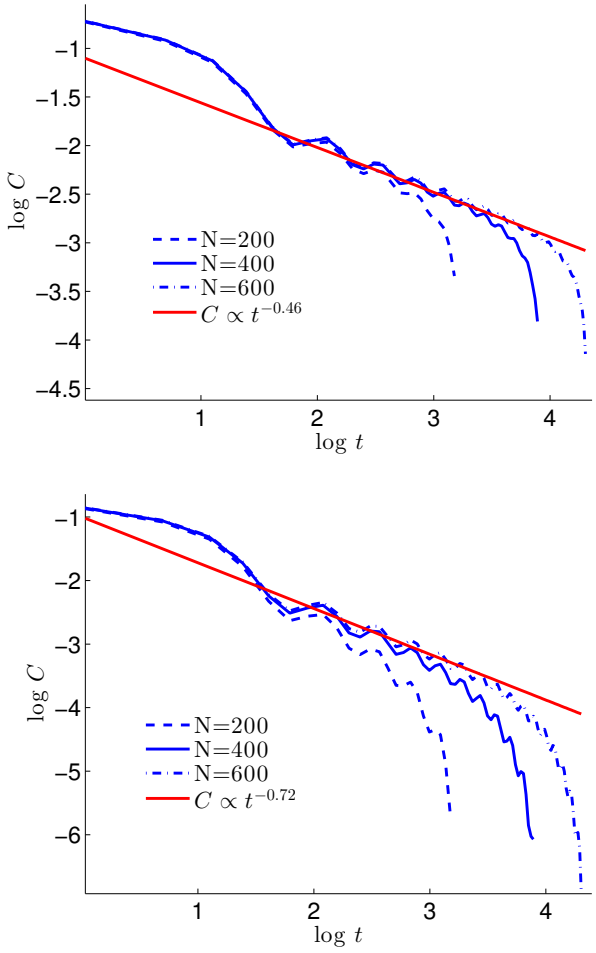

Figure 13. *Correlations in the light-cone regime.* We measure the correlations between two points in the regime described in the text as *light-cone*, with $\frac{d_{\min}}{vt} = 1/2$, $\frac{d_{\max}}{vt} = 2$ and $vt < N/2$. Upper panel: if both points are in the same half, correlations decay with time as t^{-3x} with $x = 0.46(1)$. Lower panel: if both points are in different halves, correlations decay with the same law, but $x = 0.72(1)$, close to $3/4$.

a join quench. This is not very surprising, since both quenches are globally very different. Still, we can attempt a local characterization of the equilibrium regime. Since the quenching Hamiltonian are locally identical, and the initial states provide the same correlations functions in the bulk, one might expect similar behaviors in both quenches.

The top panel of Fig. 15 shows that, as expected, after splitting or joining, local observables display all three stages, the static, the out-of-equilibrium and the equilibrium stages. The static value of the magnetization depends on the system size as

$$\langle \sigma_z \rangle_0 = \sigma_\infty + \frac{c_z}{N}, \tag{18}$$

where both σ_∞ and c_z are known analytically [58]. Let us consider the two cases of a $N = 200$ spin-chain split into two halves and two $N = 100$ chains joined in a single chain. In both cases the static values differ because of the different initial system sizes, with the split value displaying larger magnetization than the join. As expected, both values cross during the out-of-equilibrium phase, and the split equilibrium magnetization is lower than the join equilibrium magnetization. The equilibrium magnetization for the split chain converges to the static value of the two chains that have been joined, while the opposite does not happen, the equilibrium value for the joint chain is not the same as the static value of larger chain before the split. This is a finite-size effect. In the thermodynamic limit, the magnetization is the same before and after the quench in both cases. Still, for finite chains, we can distinguish both quench protocols, since

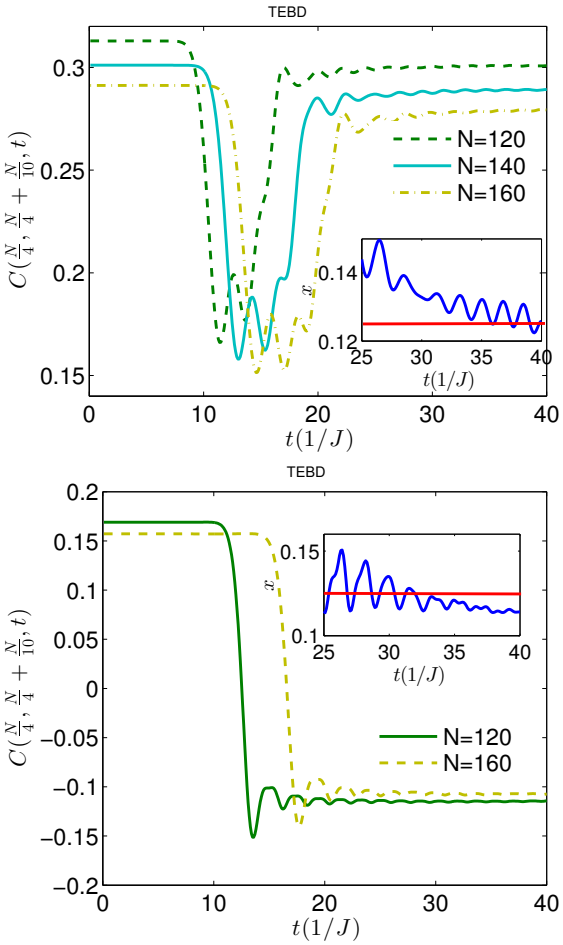

Figure 14. *Time-evolution of the correlation functions.* In the upper panel we consider the case when both points are in the same half of the chain. Concretely, we plot $C(N/4, N/4+N/10, t)$ for different chain lengths N. In both the static and equilibrium regime we observe a polynomial decay of the correlation as a function of the system size N. The critical exponent x governing the decay has been monitored as a function of time during the equilibrium regime, showing oscillatory convergence to the static value 1/8 (see inset). The lower panel shows the time evolution of the correlator when both points lie in different halves, symmetrically placed with respect to the LR interface. Concretely, we plot $C(N/2-N/10, N/2+N/10, t)$. Interestingly, the equilibrium regime leads to anti-correlation between the two half-chains, whose critical exponent x again converges through some oscillations to 1/8 (inset).

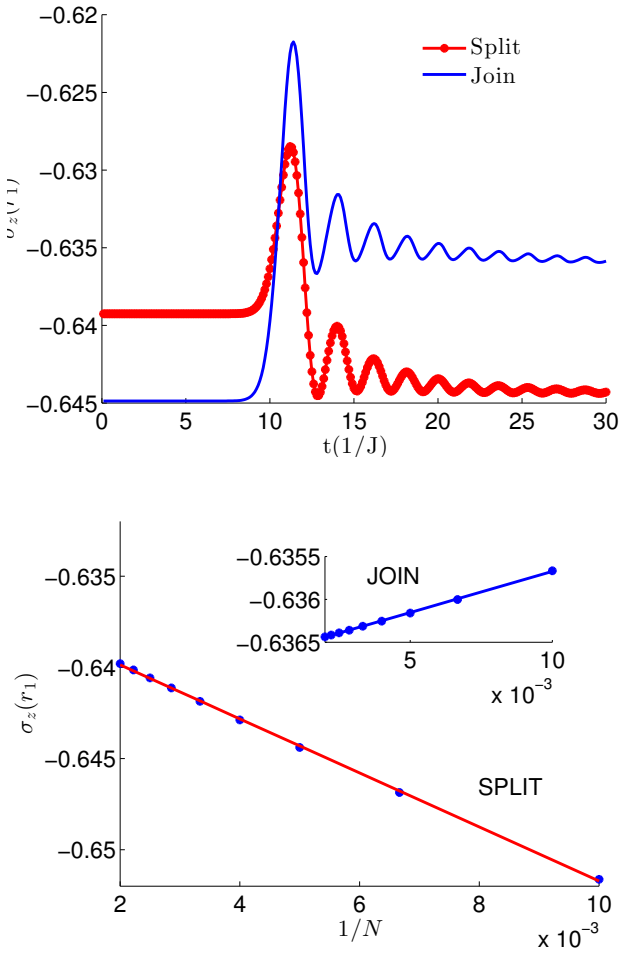

Figure 15. *Top:* Time-evolution of the expected magnetization at a site $r = N/2 - N/10$, both after a split quench of an initial chain with $N = 200$, and after a join quench of two initial chains with size 100. During the out-of-equilibrium regime, the join and the split values interchange and finally relax to different equilibrium values. *Bottom:* Scaling analysis shows that in both cases the equilibrium value is well described by Eq. 18, but the thermodynamic limit is approached from different directions, $\tilde{c}_z^{\rm split} < 0$, while $\tilde{c}_z^{\rm join} > 0$, implying that even at a local level the two quench protocols are well distinguishable.

the magnetization approaches the thermodynamic limit from opposite directions.

Indeed, as shown in the bottom panel of Fig. 15, the fit to Eq. 18 of the finite-size data shows that $\tilde{c}_z^{\rm split} < 0$ and $\tilde{c}_z^{\rm join} > 0$, implying that even at a local level the two quench protocols are well distinguishable. The same study is performed for the energy density in Fig. 16, where again we see that the quenches are completely distinguishable at a local level.

Finally we can also characterize intermediate quenches, considering a parameter $\tilde{t}$ that modifies the strength of the bond connecting L and R, as $\tilde{t} \cdot H_{LR}$(see Eq. (2)) so that the quench is obtained by varying the initial value of $\tilde{t}$. In this way we can either weaken the Hamiltonian bond between L and R by passing from the initial value of $\tilde{t} = 1$ to a quench value of $0 < \tilde{t} < 1$ so to partially split the chain. Alternatively we can quench from the initial $\tilde{t} = 0$ to again any value $0 < \tilde{t} < 1$ so to partially join L and R by switching on a weaker bond between them (weaker than the other present in the chain). The numerical results for such intermediate quenches are shown in Fig. 17 where we appreciate that by looking at the

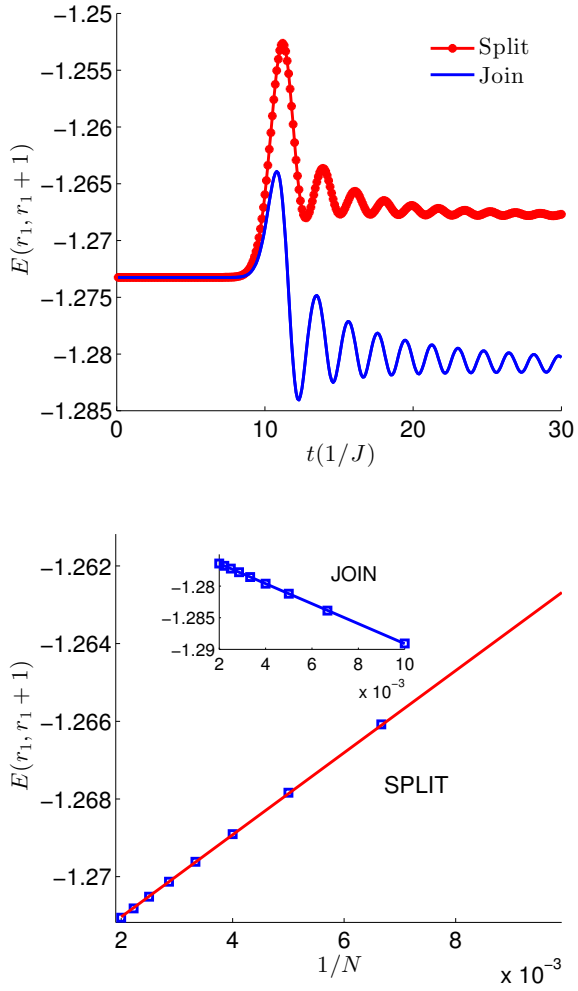

Figure 16. *Top:* Time-evolution of the expected energy at link $r_1 = N/2 - N/10$, both after a split quench of an initial chain with $N = 200$, and after a join quench of two initial chains with size 100. They relax to different equilibrium values. *Bottom:* The scaling analysis shows that in both cases the equilibrium value is the same but the thermodynamic limit is approached from different directions, implying that even at a local level the two quench protocols are well distinguishable.

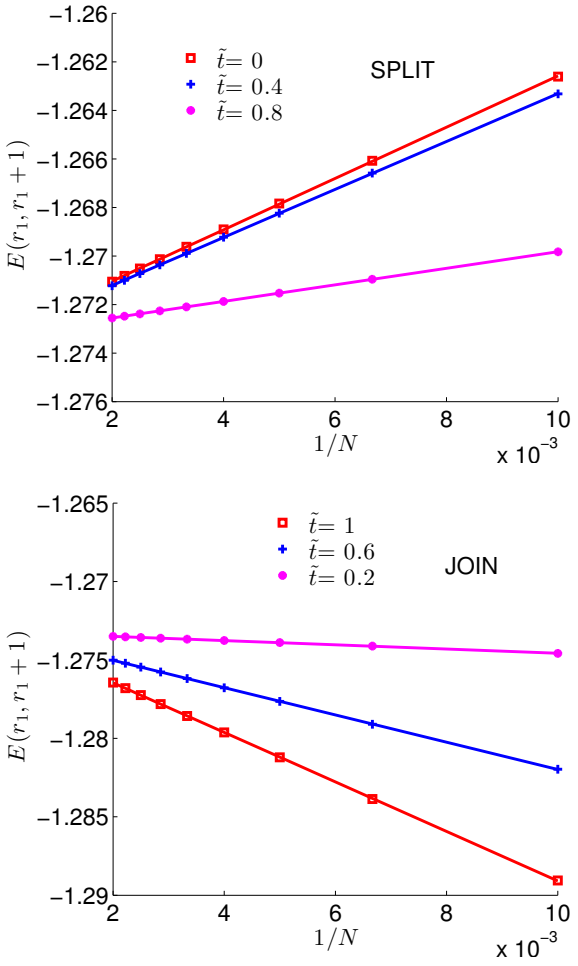

Figure 17. Intermediate quenches. The scaling of local observable with respect to the system size are presented in the equilibrium regime after either weakening the Hamiltonian between L and R so to provide a partial split of the two originally joined chains (*upper panel*) and after introducing a weak bond between L and R so to partially join the originally separated chains (*lower panel*). The slope of the finite size effects is in one to one correspondence with the strength of the Hamiltonian bond joining L and R giving the possibility to local discern all the above scenarios. We have considered $r_1 = N/2 - N/10$.

sign of the finite size corrections we can distinguish if the chain is being split (even partially) or joined. This last situation is similar to the study of the effects of impurities in critical systems [54].

IV. CONCLUSIONS AND OUTLOOK

In this work we have discussed the time evolution of a critical spin-chain which is quenched by effectively disconnecting its two halves. Due to the entanglement in the initial state each of the two halves is originally in a mixed state. The bipartite entanglement between the halves is conserved during the evolution and so is the entanglement spectrum of the bipartition. We address the role of the conservation of the ES by comparing this quench with the one where two independent spin chains are joined together. Both the initial state and the quenching Hamiltonian are locally indistinguishable in the bulk of the system away from the partition in two halves. The joining quench however, due to the interaction between the two halves, does not conserve the entanglement spectrum of the bipartition. We show that the equilibrium states emerging after the two quenches differ both globally and locally.

This suggests that the conservation of the entanglement spectrum has important consequences on both the out-of-equilibrium evolution of many-body systems and

their equilibration regime.

As opposed to other scenarios discussed in the literature, the conservation of the ES is not related to integrability of the dynamics, but rather to the specific quench protocol and the basic nature of entanglement.

The splitting of a spin chain in two halves is a local quench and as such does not inject enough energy in the system to observe thermalization at any non-zero temperature. In other terms, it can not give rise to an equilibrium state with finite entropy density.

We plan to generalize this analysis to global quenches that inject enough energy in the initial state for effective thermalization to take place an thus address which are the effects of the conservation of the entanglement spectrum also in those scenarios.

V. ACKNOWLEDGMENTS

We would like to thank P. Calabrese, M. Fagotti, E. Tonni for numerous discussions on the topic. In particular we thank M. Fagotti and A. Riera for their critical reading of a first version of our manuscript. We acknowledge financial support from the Marie Curie project FP7-PEOPLE-2010-IIF ENGAGES 273524, TOQATA (FIS2008-00784), ERC QUAGATUA OSYRIS, EU IP SIQS, and the Spanish government grant FIS2012-33642.

[1] J. von Neumann, Z. Phys **57**, 30 (1929).
[2] M. Lewenstein, A. Sanpera and V. Ahufinger, *Ultracold atoms in optical lattices*, Oxford University Press (2012).
[3] T. Kinoshita, T. Wenger and D.S. Weiss, Nature **440**, 900 (2006).
[4] M. Cheneau, P. Barmettler, D. Poletti, M. Endres, P. Schausz, T. Fukuhara, C. Gross, I. Bloch, C. Kollath and S. Kuhr, Nature **481**, 484 (2012).
[5] M. Gring, M. Kuhnert, T. Langen, T. Kitagawa, B. Rauer, M. Schreitl, I. Mazets, D.A. Smith, E. Demler and J. Schmiedmayer, Science **337**, 1318 (2012).
[6] S. Trotzky, Y.A. Chen, A. Flesch, I.P. McCulloch, U. Schollwöck, J. Eisert and I. Bloch, Nat. Phys. **8**, 325(2012).
[7] T. Langen, R. Geiger, M. Kuhnert, B. Rauer and J. Schmiedmayer, Nat. Phys. **9**, 640 (2013)
[8] J.M. Deutsch, Phys. Rev. A **43**, 2046 (1991).
[9] A. Polkovnikov, K. Sengupta, A. Silva and M. Vengalattore, Rev. Mod. Phys. **83**, 863 (2011).
[10] M. Sredniki, Phys. Rev. E **50**, 888 (1994).
[11] M. Rigol, V. Dunjko, and M. Olshanii, Nature **452**, 854 (2008); M. Rigol, Phys. Rev. Lett. **103**, 100403 (2009).
[12] E. Jaynes, Phys. Rev. **106**, 620 (1957).
[13] L.D. Landau, L.P. Pitaevskii and E.M. Lifshitz, *Statistical physics I*, Pergamon Press (1980).
[14] R.K. Pathria, *Statistical mechanics*, Butterworth-Heinemann (1996).
[15] R. Balian, *From Microphysics to Macrophysics: Methods and Applications of Statistical Physics*, Springer (2007).
[16] M. Rigol, V. Dunjko, V. Yurovsky and M. Olshanii, Phys. Rev. Lett. **98**, 050405 (2007).
[17] J. Berges, S. Borsanyi and C. Wetterich, Phys. Rev. Lett. **93**, 142002 (2004).
[18] M. Kollar, F.A. Wolf and M. Eckstein, Phys. Rev. B **84**, 054304 (2011).
[19] H. Li and F.D.M. Haldane, Phys. Rev. Lett. **101**, 010504 (2008).
[20] M. Chung, A. Iucci, M. A. Cazalilla, New J. Phys. **14** 075013 (2012). M. A. Cazalilla, A. Iucci, M. Chung, Phys. Rev. E **85**, 011133 (2012).
[21] S. Popescu, A.J. Short and A. Winter, Nat. Phys. **2**, 754 (2006).
[22] A. Riera, C. Gogolin and J. Eisert, Phys. Rev. Lett. **108**, 080402 (2012).
[23] L. Masanes, A.J. Roncaglia and A. Acín, Phys. Rev. E **87**, 032137 (2013).
[24] M. Fagotti and F.H.L. Essler, Phys. Rev. B **87**, 245107 (2013).
[25] M.B. Hastings, J. Stat. Mech.: Theor. Exp. P08024 (2007).
[26] L. Masanes, Phys. Rev. A **80**, 052104 (2009).
[27] P. Calabrese and J. Cardy, J. Stat. Mech.: Theor. Exp. P04010 (2005).
[28] P. Hauke and L. Tagliacozzo, Phys. Rev. Lett. **111**, 207202 (2013).
[29] C. Gogolin, M.P. Müller and J. Eisert, Phys. Rev. Lett. **106**, 140401 (2011).
[30] J. Schachenmayer, B.P. Lanyon, C.F. Roos and A.J. Daley, Phys. Rev. X **3**, 031015 (2013).
[31] P. Calabrese and J. Cardy, Phys. Rev. Lett. **96**, 136801 (2006).
[32] J.M. Stéphan and J. Dubail, J. Stat. Mech.: Theor. Exp. P08019 (2011).
[33] V. Eisler and I. Peschel, J. Stat. Mech.: Theor. Exp. P06005 (2007).
[34] E. Lieb, T. Schultz and D. Mattis, Rev. Mod. Phys **36**, 856 (1964).
[35] M. Fagotti and P. Calabrese, Phys. Rev. A **78**, 010306 (2008)
[36] G. Torlai, L. Tagliacozzo and G. De Chiara, J. Stat. Mech.: Theor. Exp. P06001 (2014).
[37] G. Vidal, Phys. Rev. Lett. **91**, 147902 (2003).
[38] G. Vidal, Phys. Rev. Lett. **93**, 040502 (2004).
[39] J.I. Cirac, D. Poilblanc, N. Schuch and F. Verstraete, Phys. Rev. B **83**, 245134 (2011).
[40] I. Peschel and T.T. Truong, Z. Phys. B **69**, 385 (1987).
[41] A.M. Läuchli, ArXiv: 1303.0741 (2013).
[42] G. De Chiara, L. Lepori, M. Lewenstein and A. Sanpera, Phys. Rev. Lett. **109**, 237208 (2012).
[43] V. Alba, M. Haque and A. Läuchli, Phys. Rev. Lett. **108**, 227201 (2012)
[44] C. Holzhey, F. Larsen and F. Wilczek, Nucl. Phys. B **424**, 443 (1994).
[45] C. Callan and F. Wilczek, Phys. Lett. B **333**, 55 (1994).
[46] M. Srednicki, Phys. Rev. Lett. **71**, 666 (1993).
[47] G. Vidal, J.I. Latorre, E. Rico and A. Kitaev, Phys. Rev. Lett. **90**, 227902 (2003).

[48] P. Calabrese and J. Cardy, J. Stat. Mech.: Theor. Exp. P06002 (2004).
[49] P. Calabrese and J. Cardy, J. Stat. Mech.: Theor. Exp. P10004 (2007)
[50] F. Iglói, Z. Szatmári and Y.C. Lin, Phys. Rev. B **85**, 094417 (2012).
[51] V. Eisler, D. Karevski, T. Platini and I. Peschel, J. Stat. Mech.: Theor. Exp. P01023 (2008).
[52] A.M. Läuchli and C. Kollath, J. Stat. Mech.: Theor. Exp. P05018 (2008).
[53] M. Collura and P. Calabrese, J. of Phys. A: Math. Theor. **46**, 175001 (2013).
[54] V. Eisler and I. Peschel J. Stat. Mech. : Theor. Exp. P04005 (2014).
[55] V.Alba and F. Heidrich-Meisner arXiv:1402.2299.
[56] Á. Perales and G. Vidal, Phys. Rev. A **78**, 042337 (2008).
[57] U. Divakaran, F. Iglói and H. Rieger, J. Stat. Mech.: Theor. Exp. P10027 (2011).
[58] T.W. Burkhardt and I. Guim, J. Phys. A: Math. Gen. **18**, L33 (1985).

Appendix A: Profile of the entanglement entropy

We guess from our numerical data the following functional form for the projection of the entanglement entropy $S(r,t)$ over space or time discussed in Sect. IIIB:

$$\tilde{S}_X(x) = \frac{c}{\alpha_x} \log_2 \left| \frac{N}{\pi} \left(\sin \frac{2\pi x}{T_x} \right)^{\nu_x} \right| + \text{cst.} \qquad \text{(A1)}$$

In this way by either chosing $x = r$ or $x = t$ we recover both space and time sections of the entanglement entropy that are presented in Fig. 8. In each case T_x has to be chosen accordingly to the definition discussed in the next paragraph.

$$\begin{aligned} x = r &\to \tilde{S}_X(x) = \tilde{S}_S(r) \\ x = t &\to \tilde{S}_X(x) = \tilde{S}_T(t) \end{aligned} \qquad \text{(A2)}$$

- **Calculation of the parameter α_x.** We first determine the value of α_x in both cases. α_x is extracted through a finite size scaling analysis. By fxing the ratio $\frac{t}{N}$, we study how Eq. (A1) depends on N since $\tilde{S}_X(x) = \frac{c}{\alpha_x} \log_2 N + \text{cst}$. Specifically the calculation has been done using chains with $N = 100, 120, 140, 160, 200, 240$.

  For the case of $\tilde{S}_T(t)$ we have considered ratios

  $$\frac{t}{N} = \frac{1}{2} \cdot \left(\frac{2}{10}, \frac{3}{10}, \frac{5}{10}, \frac{6}{10} \right), \qquad \text{(A3)}$$

  while for $\tilde{S}_S(r)$ we have considered sites $r \ll N/2$ and ratios

  $$\frac{t}{N} = \left(\frac{2}{10}, \frac{3}{10}, \frac{4}{10}, \frac{6}{10}, \frac{7}{10} \right). \qquad \text{(A4)}$$

  Averaging on the values of α extracted from the various ratios we obtain

  $$\begin{aligned} \tilde{S}_T(t) &\to \alpha_T = 2.919\ (41) \\ \tilde{S}_S(r) &\to \alpha_S = 2.947\ (13) \end{aligned} \qquad \text{(A5)}$$

  that are both compatible with $\alpha = 3$. In order to cross-check our strategy we have repeated the same procedure for the join quench. In this case we obtain

  $$\begin{aligned} \tilde{S}_T(t) &\to \alpha_{join} = 3.012\ (59) \\ \tilde{S}_S(r) &\to \alpha_{join} = 3.042\ (10) \end{aligned} \qquad \text{(A6)}$$

  that is in agreement with the available theoretical prediction $\alpha_{join} = 3$ [32, 49, 50].

- **Calculation of the parameter ν_x.**

At fixed N, $\tilde{S}_X(x)$ depends linearly on $y = \log_2 \left| \left(\sin \frac{2\pi x}{T_x} \right) \right|$. We can thus extract the value of ν_x throug a linear fit of $\tilde{S}_X$ as a function of y at fixed N. We have performed such analysis for several chains of length $N = 100, 120, 140, 160, 200, 240$ obtaining several estimates of ν_x.

In particular for $\tilde{S}_T(t)$, $T_x = N$, and for each N we have considered the set of times

$$t = \left(\frac{N}{8}, \frac{N}{8} + 1, ..., \frac{N}{2} - \frac{N}{8} \right). \tag{A7}$$

For $\tilde{S}_S(r)$, $T_x = 2N$ and we have considered $r \ll N/2$:

$$r = \left(\frac{2N}{10}, \frac{2N}{10} + 1, ..., \frac{N}{4} \right) \tag{A8}$$

Averaging on the values of ν obtained for each N we get

$$\tilde{S}_T(t) \to \nu_T = 0.500\ (14) \tag{A9}$$

$$\tilde{S}_S(r) \to \nu_S = 1.004\ (5) \tag{A10}$$

While the first result is un-expected, the second is compatible with what expected in a join quench. By repeating the analysis for the join quench where we expect $\nu_{join} = 1$ [32, 49, 50] we indeed find

$$\tilde{S}_T(t) \to \nu_{join} = 0.975\ (34)$$

$$\tilde{S}_S(r) \to \nu_{join} = 1.070\ (10) \tag{A11}$$

as expected.